Advances in simultaneous salt boundary and background tomography updating

Taylor Dahlke, Biondo Biondi and Robert Clapp

ABSTRACT

Level set methods can provide a sharp interpretation of the salt body by defining the boundary as an isocontour of a higher dimensional implicit representation, and then evolving that surface to minimize the Full Waveform Inversion (FWI) objective function. Because the implicit surface update gradient is based on the tomographic update gradient, there is potential to utilize it to update the background velocity concurrently with the salt boundary. Using a shape optimization approach on synthetic examples, we can achieve reasonable convergence both in terms of the residual L2 norm, as well as the evolution of the salt boundary and background velocity towards the true model, demonstrating the feasibility of this approach. Various factors in processing the gradients and calculating step size influence this convergence, which we analyze and address. Ultimately, this method can be integrated into the processing work flow as a tool that provides improved building and refining of the velocity models used for imaging.

INTRODUCTION

Tomographic approaches to interpreting salt bodies can be less than effective, because the results tend to be too smooth to provide significantly accurate placement of salt boundaries. Manual and semi-automatic picking of salt boundaries is a common approach to interpreting the desired sharp delineations, but these methods can be time-consuming and tedious since expert input is necessary for either the actual picking, or the oversight and correction. Furthermore, once a model has been produced, it must be used to generate an image, and then be refined as necessary. A robust method for further automating the salt interpretation procedure would greatly alleviate this bottleneck.

Some previous approaches to interpreting salt boundaries use a shape optimization approach (Guo and de Hoop (2013), Lewis et al. (2012)). The boundaries of a salt body can be represented as the zero-isocontour of a higher dimensional surface (for example, a 2D boundary as a contour of a 3D surface). A gradient can be derived to evolve this shape / isosurface according to the FWI objective function. Unlike the smooth boundaries produced by tomographic approaches, the isocontour resulting from the shape optimization provides a sharp boundary, which is a more appropriate way to classify most salt-sediment interfaces. Guo and de Hoop (2013)

utilize this approach using a frequency domain forward wave operator to evolve a salt boundary and velocity model. However, their approach alternates between updating the background velocity and salt body boundary, which effectively requires twice as many iterations as performing both updates concurrently.

The approach we take utilizes shape optimization with the use of time domain forward wave-propagation, which allows us to take advantage of using a continuous range of frequencies (rather than discrete frequencies) in each iteration, allowing for sharper delineation of the boundary. Further, we take advantage of the fact that our boundary update gradient is based on the tomographic update gradient, and make updates to both concurrently after applying optimal scaling parameters. In theory, this method has the potential to be more efficient than an alternating update approach. In this paper we will discuss the fundamentals of the level set method and its key properties, followed by a demonstration of the concurrent boundary-tomography update method on a test model, as well as discussion on how we address the challenges inherent with concurrent updating.

THEORY

We begin with a brief overview of the level set method and how we apply the evolution scheme it utilizes. The full derivation for the shape optimization implementation can be found in Dahlke (2014).

Level set fundamentals

In our problem, we are trying to determine the boundary of a two dimensional body. Instead of using an algorithm that operates in this 2D plane directly, we use the level set algorithm which evolves a 3D implicit surface, ϕ. While our algorithm acts directly on this surface instead of the boundary, our solution for the 2D boundary is simply represented by a contour "slice" of this implicit surface where $\phi = 0$, as described in Osher and Sethian (1988) and Burger (2003). While it may seem counterintuitive to add extra dimensionality to our problem, by doing so we gain some advantages. These include the ability to merge and separate bodies as the level set evolution proceeds, as well as the ability to handle sharp corners and cusps in the lower-dimensional (2D) plane that the boundary exists on.

Based on this concept, we define a spatial domain $\Theta \subset \mathbb{R}^2$, a (salt) body $\Omega \subset \Theta$, and the salt body boundary Γ such that

$$\Omega = \{x \mid \phi(x,\tau) > 0\}, \qquad \Gamma = \{x \mid \phi(x,\tau) = 0\},$$

where τ indicates the axis along which the evolution steps progress ($\tau = 0$ is the initial iteration). As such, for a single step along τ, our salt body Ω evolves to $\Omega^{'}$.

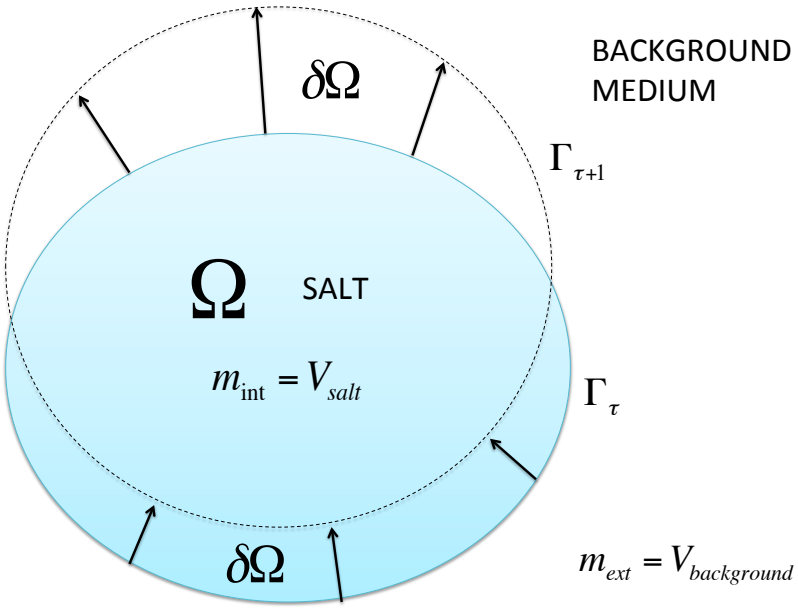

Figure 1: Diagram of domain partitioning. The full inclusive domain is Θ. Ω is the salt body. $\partial\Omega$ is the difference between the salt body domain in iteration τ and iteration $\tau + 1$. Γ is the boundary of the salt body, with the subscript τ indicating the iteration. [**NR**]

We define a point along the boundary curve to be

$$x_\Gamma = \{x \in \Gamma\}.$$

With this definition of the boundary points, the level set of ϕ that represents the salt body boundary can be described as

$$\phi(x_\Gamma, \tau) = 0.$$

By taking the derivative of this equation, the chain rule gives us

$$\frac{\partial \phi}{\partial \tau} + \frac{\partial \phi}{\partial x_\Gamma}\frac{\partial x_\Gamma}{\partial \tau} = 0. \tag{1}$$

This equation can be readily rewritten as

$$\frac{\partial \phi}{\partial \tau} + \vec{\nabla}\phi \cdot \vec{v}(x_\Gamma, \tau) = 0. \tag{2}$$

We can use $\vec{\nabla}\phi$ defined over all the full domain of x (rather than just x_Γ) since $\vec{\nabla}\phi \cdot \vec{v}(x_\Gamma, \tau)$ is a dot product, and only the terms where $x \in \Gamma$ will contribute to the overall dot product result. This "velocity" term in equation 2 can be defined as having both a "speed" and a normal vector component, $\vec{v}(x_\Gamma, \tau) = V(x_\Gamma, \tau)\vec{n}(x_\Gamma, \tau)$. In complete form there is also a tangential component, but we ignore this part since it doesn't contribute to a change in the surface ϕ.

We know the normal vector is defined as

$$\vec{n}(x_\Gamma, \tau) = \frac{\vec{\nabla}\phi(x_\Gamma, \tau)}{|\vec{\nabla}\phi(x_\Gamma, \tau)|} \ ,$$

which allows us to restate equation 2 in a more familiar representation

$$\frac{\partial \phi}{\partial \tau} = -V(x_\Gamma, \tau)\,|\nabla \phi|\,. \tag{3}$$

The scalar speed term $V(x_\Gamma, \tau)$ describes the magnitude of the variation of ϕ that is normal to the boundary Γ. It determines the evolution of the implicit surface, and ultimately the boundary implied by it. This term can be found to be

$$\frac{\partial \phi}{\partial \tau} = -\sum_s \int_0^T \int_{x\in\Gamma} (q_1^2 - q_2^2) h_s(x,t) \frac{\partial^2 u_s(x,t)}{\partial t^2} d\sigma dt\,|\nabla \phi|\,, \tag{4}$$

as described in the derivation provided in Dahlke (2014), which demonstrates how this formulation of the scalar speed term directs the evolution of the implicit surface such that it minimizes the FWI objective function. An important insight from this referenced derivation is that the scalar speed term contains the tomographic update gradient within it

$$-\sum_s \int_0^T \int_{x\in\Gamma} h_s(x,t)\frac{\partial^2 u_s(x,t)}{\partial t^2} d\sigma dt, \tag{5}$$

We can take advantage of it already being calculated and use it to make updates to the background velocity. In the following section we demonstrate this implementation approach.

APPLICATION ON SYNTHETIC EXAMPLES

We demonstrate the shape optimization algorithm on a 2D model, with the implicit surface evolved being a 3D surface. In this section we describe the algorithm used and the results that have come from its implementation.

Evolution algorithm

We begin with an initial background velocity, and a binary function as the initial implicit surface ϕ. Since we assume a constant salt velocity, we use both of these inputs to create a full initial-guess velocity model (m_o). Using this m_o, we forward model to get our d_{syn} which we use to get a residual. The residual is used to calculate both a tomographic and a boundary update gradient, as described in the derivation provided in Dahlke (2014). We then perform forward linearized operations on these gradients so that we can do a linear plane search (in residual space) for the scaling parameters α and β. Following this, we do a non-linear line search for a γ parameter that rescales α and β in a manner that minimizes the FWI objective function. We then apply an explict forward Euler scheme that updates the implicit surface (ϕ) and the background velocity V_{back}. This workflow is outlined in algorithm 1.

$$\phi^{j+1} = \phi^j + \gamma(\beta\frac{\partial\phi}{\partial j} + \mu G_{\text{reg}}), \tag{6}$$

$$V_{\text{back}}^{j+1} = V_{\text{back}}^j + \gamma\alpha\frac{\partial V_{\text{back}}}{\partial j}, \tag{7}$$

where β and α are the step sizes (for tomography and salt boundary respectively) and j is the current iteration point.

Algorithm 1 Shape optimization and tomographic update algorithm

Load observed data d_{obs}
Load initial implicit surface ϕ
Load background velocity V_{back}
for $i = 0$ to *numiter* **do**
  Build full velocity model V_{full} from ϕ and V_{back}
  Forward model $\rightarrow d_{syn}$
  Calculate data space residuals ($r = d_{syn} - d_{obs}$)
  Perform direct arrival mute on residuals
  Back-propagate residuals (RTM imaging) $r \rightarrow \partial V_{full}/\partial i$
  Calculate $\nabla\phi$
  Calculate $\partial\phi/\partial i$
  Mute and smooth $\partial V_{full}/\partial i$
  Forward model $\partial\phi/\partial i \rightarrow d_{bound}$
  Forward model $\partial V_{full}/\partial i \rightarrow d_{tomo}$
  Peform linear plane search for α and β
  Perform non-linear plane search for γ
  Update boundary: $\phi^{i+1} = \phi^i + \gamma\beta\frac{\partial\phi}{\partial i}$
  Update background velocity: $V_{back}^{i+1} = V_{back}^i + \gamma\alpha\frac{\partial V_{full}}{\partial i}$
end for
Output final velocity model

Scaling parameter optimization

As shown previously, the salt boundary update gradient is based on the adjoint of the linearized-Born operator, which is the tomographic update gradient. Since the gradient for both a tomographic and boundary update are calculated in each step regardless, we attempt to take advantage of this by finding scaling parameters to apply to these gradient updates such that we minimize the residual space objective function

$$\min_{\alpha,\beta} \left\| FG_{\text{tomo}}^T\alpha + FG_\phi^T\beta - (d_{\text{calc}} - d_{\text{obs}}) \right\|, \tag{8}$$

where F is the forward wave propagator, and G_{tomo}^T and G_ϕ^T are the update gradients for the background velocity and implicit surface ϕ respectively.

Minimizing this objective function gives us parameters that are scaled to the residual space, not the gradient space where they are actually applied. Since the adjoint operator that we use creates a scaling difference between the residual and gradient (data and model) spaces, we must rescale α and β once they are found so that they can be effectively applied to the gradients.

The approach we use is to rescale α and β according to a γ parameter which

is found using a non-linear line search (which is constrained by the conditions for stability). This technique is much cheaper than performing a full non-linear plane search for α and β, but still allows for a choice of parameters based on the FWI objective function. We choose this approach, utilizing equation 9 for a line search for γ,

$$\min_{\gamma} \|F(m(\gamma) - d_{\text{obs}})\| \,. \tag{9}$$

Tomographic gradient masking and smoothing

The separation of the tomographic information from the reflectivity information is desired so that the tomogaphic updates more quickly lead to convergence of the true solution. This seperation can be better achieved prior to this search for the scaling parameters by masking out the tomographic update gradient in areas where the update has no influence on changing the next iteration of the velocity model. For example, in this work we assume a constant velocity throughout the salt bodies we model. Because of this, we dont apply the tomographic gradient update in the regions where salt exists. If we calculate G^T_{tomo} without first masking out G_{tomo} in areas overlapped by salt regions, then we introduce bias into the objective function (equation 8), since it will optimize for an update that will not be entirely applied.

We further assume that the salt boundary change will not undergo significant shifts. With this in mind, we apply the masking based on the salt body delineation that was created from the most recent (previous) iteration. Another approach would be to dynamically update the salt boundary based on the scaling parameter β, as β is being solved for. While theoretically producing a more accurate update, this method is also far more expensive, since numerous applications of the forward linearized-Born operator are necessary. For this reason we make the approximation of masking based on the previous iteration of the salt boundary.

When the masking is performed and the salt boundary shrinks, an area of the background velocity is exposed which contains a sharp boundary between the newly "exposed" region and the region that was previously exposed and updated. This can create false (albeit weak) reflectors around the edge of the salt, causing errors as the evolution of the salt boundary continues. For this reason, immediately after masking is performed on the tomographic gradient, a smoothing operator is applied to remove sharp discontinuities in the velocity update along this boundary. Because the tomographic update information tends to be lower frequency than reflection information, this step also helps separate reflection and tomographic information by acting as a low-pass filter.

Stability

As the implicit surface is evolved, it is important to maintain stability of the evolution. One relevant aspect of maintaining stability is keeping the implicit surface update step size (β) small enough to satisfy the Courant-Friedrich's-Levy (CFL) condition, which is stated by Chaudhury and Ramakrishnan (2007) (when applied to level set evolution) as being

$$G_{\max} \cdot \gamma\beta \leq \min(h_x, h_y), \tag{10}$$

where h_x and h_y are the grid spacing in the x and y directions, and $G_{\max}$ is the maximum value of the update gradient. While later we describe how a plane search is used to determine the scaling parameters α and β, our algorithm adjusts these scaling parameters (while maintaining their ratio) in such a manner that satisfies the constraint in equation 10.

An additional measure taken to ensure the stablity of evolution is the use of a regularization term that is scaled and added to the boundary gradient before each update is applied. In this case, a distance regularization term was used. This term drives the spatial gradient of the implicit surface towards either one or zero ($\nabla\phi = \{1, 0\}$).

When irregularities begin to occur in the implicit surface during level set evolution, numerical errors start to occur which can lead to instability. By regularizing the gradient of the implicit surface as it evolves, we minimize irregularities and are able to continue evolution without having to reinitialize a signed-distance function to the salt boundary contour. An excellent reference on this type of regularization is Li et al. (2010).

Results

We apply our algorithm on a simple velocity model, using an acquisition geometry of 32 shots spaced 110 [m] apart, and 63 receivers spaced 50 [m] apart. In the example shown in Fig. 2, the initial and true background velocity models differed by up to 100 [m/s] (see Fig. 5). A bottom reflector and positive velocity gradient provides better illumination along the bottom and flanks of the circular salt body, which has a velocity of 4500 [m/s]. A stencil radius of five was used for smoothing of the tomographic update gradient prior to its application.

DISCUSSION

One thing to note when observing the trend in Fig. 4 is that the objective function does not decrease monotonically, and in some cases increases slightly. The non-linear

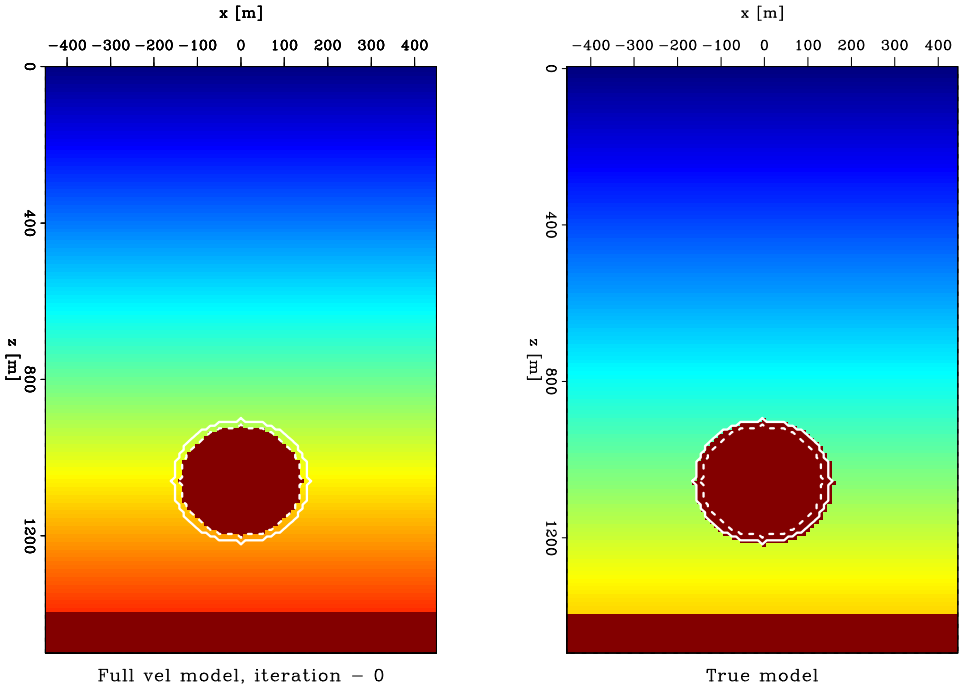

Figure 2: Initial velocity model (left) and true velocity model (right). True model boundary indicated (solid line); Initial boundary guess (dashed line). [**ER**]

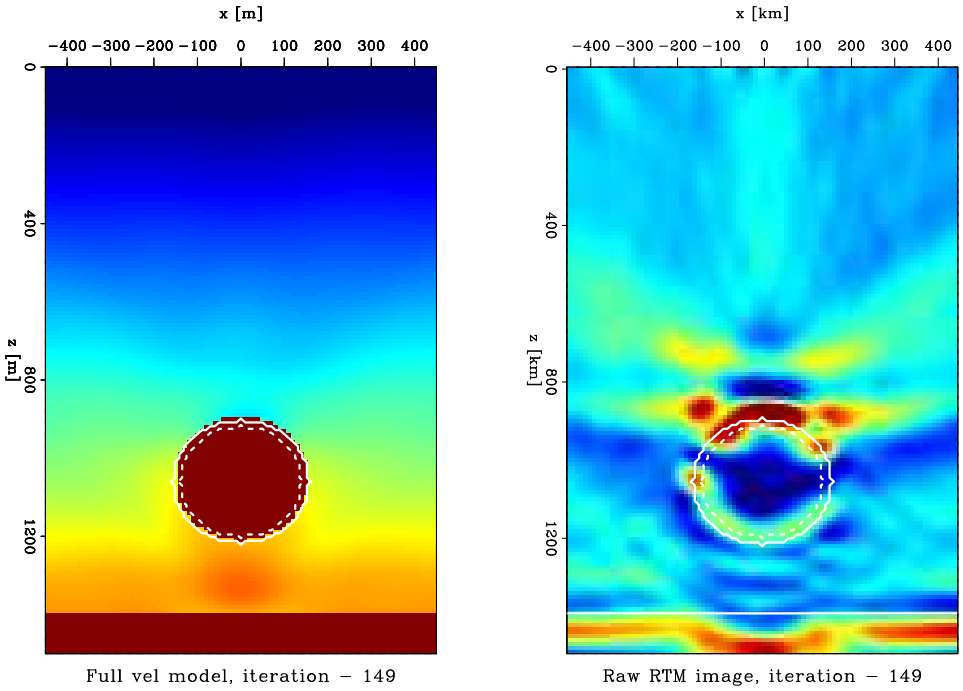

Figure 3: Final velocity model (left) and raw RTM image (right) after 149 iterations. [**ER**]

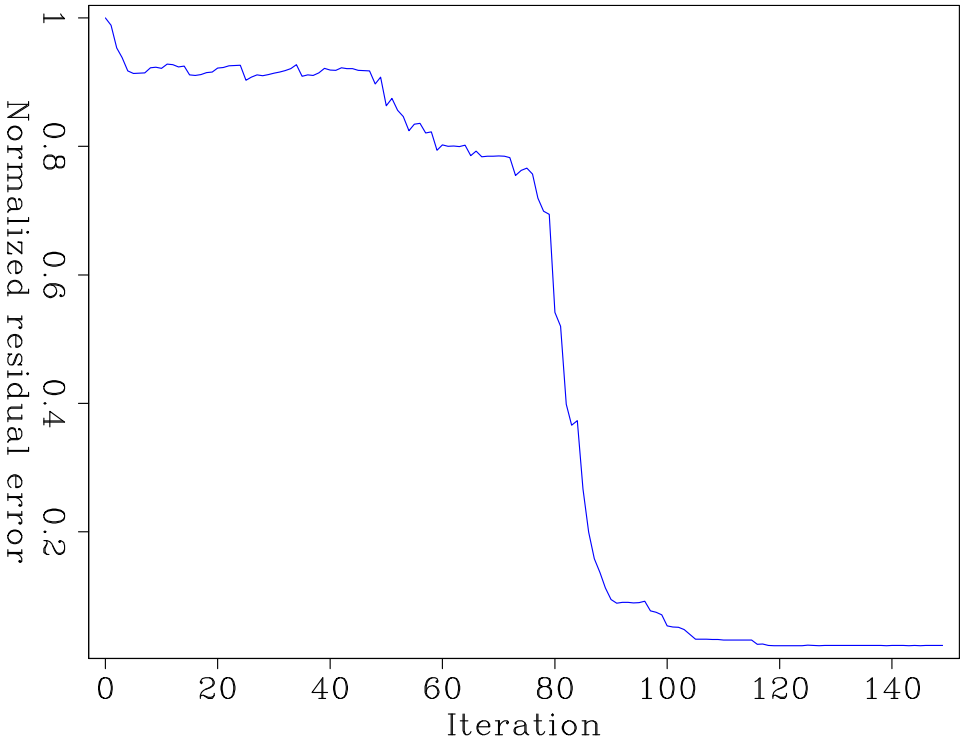

Figure 4: Objective function for evolution shown in Fig. 2 [**ER**]

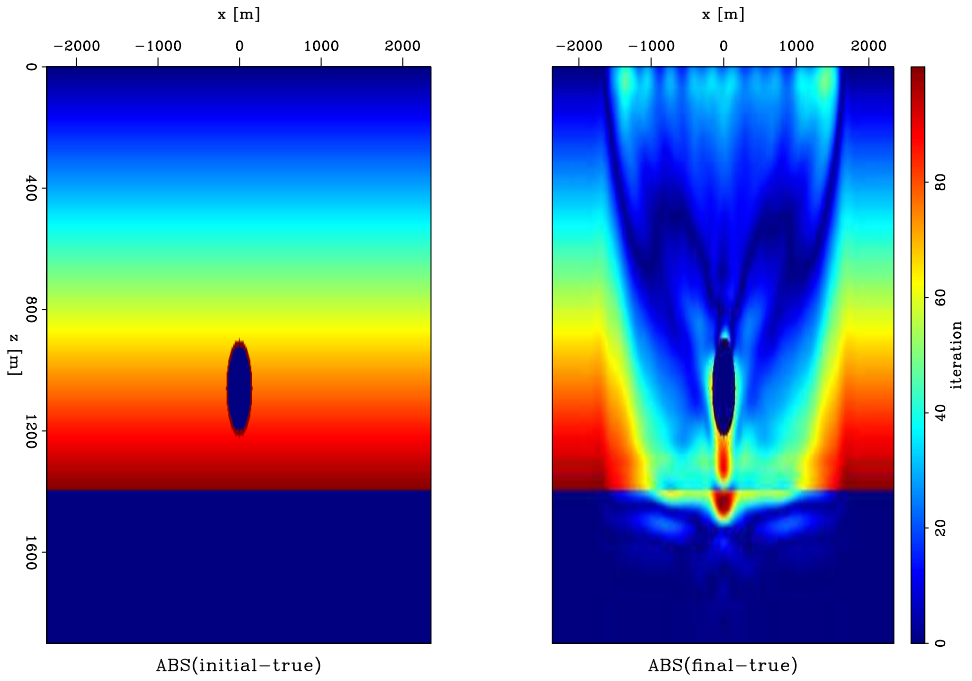

Figure 5: Change in the velocity difference for the model shown in Fig. 2 [**ER**]

line search for γ finds a minimum to the objective function by doing a quadratic interpolation between the three points surrounding the working minimum. This approximation is done for efficiency since the non-linear calculation for each point is relatively expensive, so a relatively low density of sampling along the γ axis is done. Because of the error inherent in this approximation, the algorithm may find a step size that increases the objective function slightly rather than choose a step size equal to zero.

Another observation is that the objective function plateaus at a solution that has a very low residual error, but is not the correct answer, indicating the algorithm has converged on a local minima (Fig. 4). A number of characteristics of the algorithm play into this. One is the masking operation that is performed on the tomographic update gradient. The RTM imaging places energy for the updates based on both reflection and tomographic discrepancies in the model. This mixing of reflection and tomography information is inherent to the concurrent updating approach. Even when the salt boundaries come quite close to the true position, the imaging may place energy inside the salt body region (See Fig. 3), which is never translated into a model update due to the assumption of constant velocity salt. In a model such as the one demonstrated on, the paucity of non-salt reflectors exasperates this problem and leads to convergence at a local minima solution, since some of the strongest updating energy is masked over during updating.

A further challenge demonstrated in this model is the lack of updating directly along the bottom reflector (See Fig. 3). One explanation for this is the band-limited nature of the experiment. Because the reflector acts as a step function in velocity space, in order to perfectly resolve it all frequencies must be available. Of course, our experiment uses a source wavelet centered at 15 Hz, which means our imaging will not be able to resolve this boundary to satisfaction unless more high frequencies are included.

The density of acquisition and geometry of the array also influence the number and strength of RTM imaging artifacts, which also influences the rate and quality of convergence. While a higher density of acquisition will typically lead to fewer artifacts and smoother tomographic updates, the smoothing of the tomographic update gradient also simulates that effect and is more computationally efficient. Figures 6 and 7 show that using a longer stencil length allows for quicker convergence, and also a better match to the true model. However, this approach has its limitations, and can reduce the ability of the algorithm to resolve sharper tomographic anomalies, exasperating the problems created by the band limited nature of our experiment.

CONCLUSION

In this work we described the derivation of the level set method as applied to the minimization of the FWI objective function. We demonstrated the application of this evolution algorithm and its incorporation with a background velocity tomographic

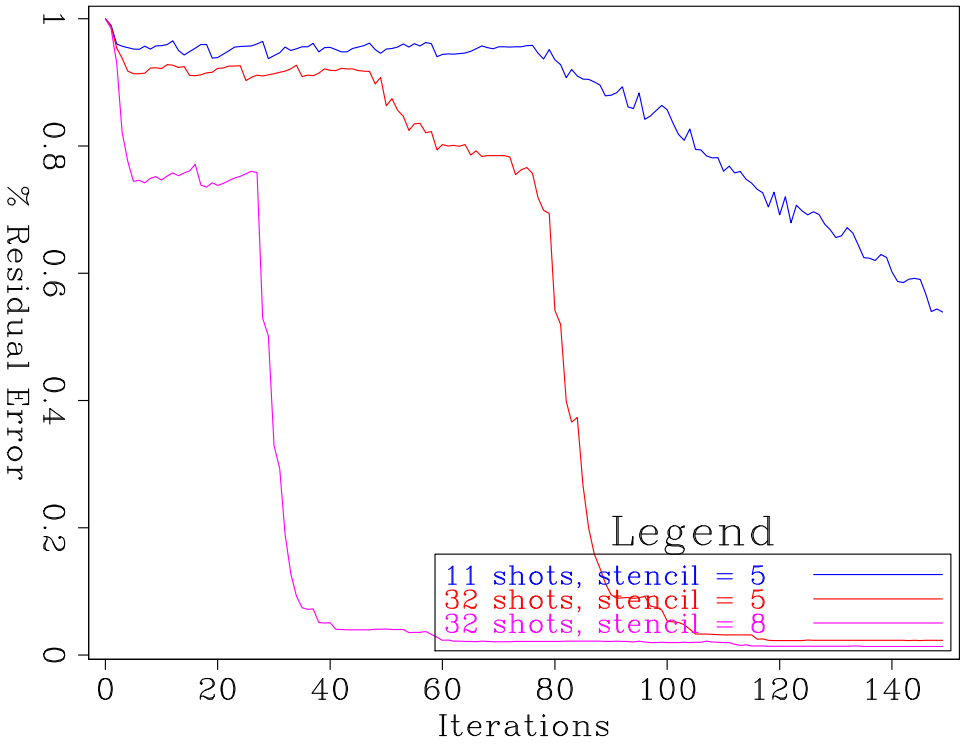

Figure 6: Different rates of convergence using the same model from Fig. 2 [**ER**]

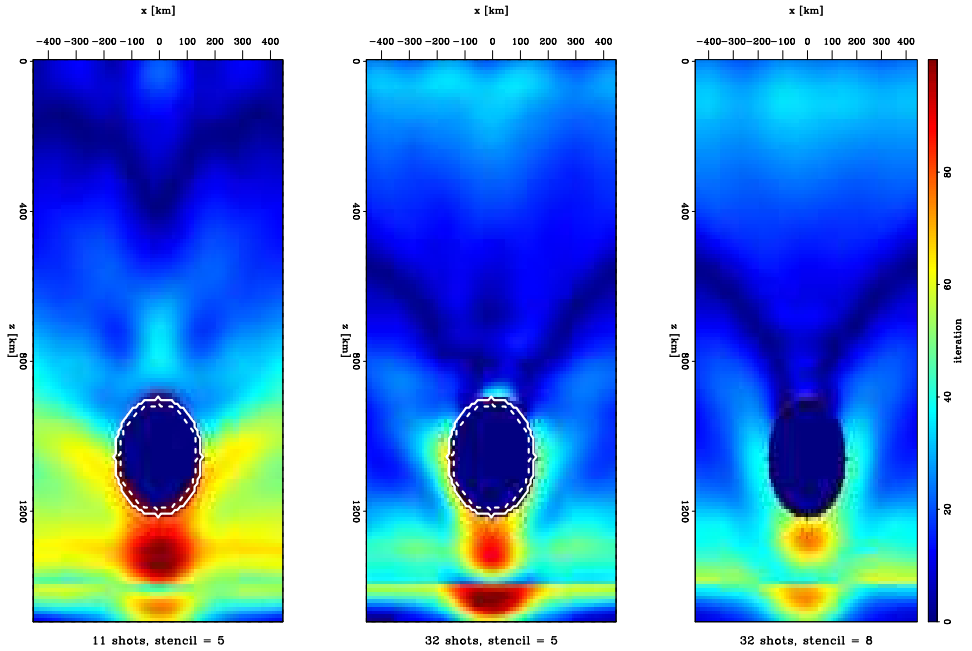

Figure 7: The absolute value of the difference between the true model and the final solution $\|V_{true} - V_{final}\|$ for varying smoothing stencil lengths and array densities. [**ER**]

update on a simple model. We consider the limitations of this approach in regards to numerical stability, as well as the assumptions of linearity that we use to find our scaling parameters, and the challenges regarding the separation of reflection information from the tomographic updating.

ACKNOWLEDGEMENTS

I would like to thank Adam Halpert, Ali Almomin, Musa Maharramov, Sjoerd de Ridder, and Stew Levin for their insight into this work. Further, I thank the SEP sponsors for their generous financial support of this research.

REFERENCES

Burger, M., 2003, A framework for the construction of level set methods for shape optimization and reconstruction: Interfaces and Free boundaries, **5**, 301–330.

Chaudhury, K. N. and K. R. Ramakrishnan, 2007, Stability and convergence of the level set method in computer vision: Pattern Recogn. Lett., **28**, 884–893.

Dahlke, Biondi, C., 2014, Shape optimization using the fwi objective function for salt body segmentation: SEP-152, 29–44.

Guo, Z. and M. de Hoop, 2013, Shape optimization and level set method in full waveform inversion with 3d body reconstruction: SEG Technical Program Expanded Abstracts, 1079–1083.

Lewis, W., B. Starr, D. Vigh, et al., 2012, A level set approach to salt geometry inversion in full-waveform inversion: Presented at the 2012 SEG Annual Meeting.

Li, C., C. Xu, C. Gui, and M. Fox, 2010, Distance regularized level set evolution and its application to image segmentation: Image Processing, IEEE Transactions on, **19**, 3243–3254.

Osher, S. and J. A. Sethian, 1988, Fronts propagating with curvature-dependent speed: algorithms based on hamilton-jacobi formulations: Journal of computational physics, **79**, 12–49.